Astron. Astrophys. 361, 273–282 (2000)

ASTRONOMY AND ASTROPHYSICS

The polarized spectrum of the dust producing Wolf-Rayet+O-star binary WR137

T.J. Harries[1], **B.L. Babler**[2], **and G.K. Fox**[2,3]

[1] University College London, Department of Physics and Astronomy, Gower Street, London WC1E 6BT, UK
[2] University of Wisconsin, Space Astronomy Laboratory, Madison, WI 53706-1390, USA
[3] King Edward VI High School, Physics Department, Morpeth, Northumberland, UK

Received 30 March 2000 / Accepted 10 July 2000

Abstract. We present high signal-to-noise, multi-epoch linear spectropolarimetry of the dust producing Wolf-Rayet+O star binary WR137 obtained over the period 1993–1998 at the William Herschel Telescope and the Pine Bluff Observatory. These observations display the 'line effect' (a reduction in polarization magnitude through the emission lines) which is an unambiguous signature of Wolf-Rayet wind asphericity. We estimate the foreground polarization by fitting the spectra with a Serkowski law plus straight-line continua. The continuum polarization magnitude is variable (although we find no correlation with binary phase), while the position angle of the intrinsic vector is remarkably constant. It is shown that the position angle of the intrinsic polarization is perpendicular to the extended dust emission observed by Marchenko et al. (1999).

Numerical simulations of electron and dust scattering in WR137 are presented. It is shown that the deviations from spherical symmetry caused by wind-wind interaction in the binary are insufficient to explain the observed polarization variability, and that the lack of polarization attributable to the dust formation episode places a strong constraint on its location.

Key words: stars: Wolf-Rayet – stars: mass-loss – stars: individual: WR137 – polarization

1. Introduction

Wolf-Rayet (WR) stars are the highly evolved descendants of massive OB stars. The spectra of WR stars exhibit the intense, broad emission lines of highly ionized species which are the signature of a hot, dense stellar wind. Analysis of recombination line diagnostics indicate that mass-loss rates are typically $\sim 10^{-5}\,\mathrm{M}_{\odot}\,\mathrm{yr}^{-1}$. WR stars may be separated into two broad classes: those in which the emission lines of nitrogen dominate (the WN stars) and those in which the carbon lines are strongest (WC stars). These two classes may then be further divided according to spectral excitation. Recent reviews of WR stars from observational and modelling perspectives are given by Willis (1999) and Crowther (1999) respectively.

Send offprint requests to: T.J. Harries (th@star.ucl.ac.uk)

Time-series photopolarimetry of WR stars has revealed that a large number of them are intrinsically polarized. Drissen et al. (1987) presented linear polarization measurements of a complete sample of Southern Galactic WN stars, all of which show evidence for an intrinsic polarization, with fluctuations of $\Delta P = 0.15\%$–0.6%. It was suggested that these fluctuations were the result of electron scattering by density inhomogeneities or 'blobs' passing through the wind. Time-series polarimetry of seven bright Cygnus WR stars (not including the binary V444 Cyg) revealed low-amplitude polarization variability (Robert et al. 1989). Similar variability was observed in photopolarimetric time-series of southern-hemisphere WC stars (St.-Louis et al. 1987).

In the case of the optically thick WR winds, the continuum forming region is located in the wind, but within the electron scattering depth unity boundary ($\tau_{es} = 1$). The emission line forming regions are located outside the continuum forming region, and usually outside the $\tau_{es} = 1$ boundary, although the radius of formation depends on the ionic species (with lines of more highly ionized species forming at smaller radii). Hence the continuum is polarized by electron scattering, but the line polarization is essentially unpolarized. If the wind is circularly symmetric with respect to the observer's sightline then the polarization from different parts of the wind cancels, and no nett polarization is observed. If, however, the wind geometry departs from projected circular symmetry (e.g. disk structures, plumes) then a small, but measurable polarization results. The magnitude of the intrinsic polarization vector decreases at the emission-line wavelength, as the unpolarized emission-line flux dilutes the polarized continuum flux. Spectropolarimetric measurements therefore provide a diagnostic probe of the three-dimensional wind geometry on spatial scales that are unresolvable using current imaging and interferometric techniques.

The first detection of such structure in the polarization spectrum of a WR star was by McLean et al. (1979) who obtained narrow-band filter polarimetry of the peculiar WN5 star EZ CMa. The depolarization was found to be a function of ionic species, with He II recombination lines less depolarized than the He I lines. The WN6 star WR134 also shows the line effect, and a comprehensive study (Schulte-Ladbeck et al. 1992) showed that

the magnitude of the continuum polarization declined through the optical region.

Schulte-Ladbeck (1994) presented a spectropolarimetric survey of Southern-hemisphere WR stars, while Harries et al. (1998, hereinafter Paper I) presented a spectropolarimetric survey of Northern hemisphere WR stars, and demonstrated statistically that 15–20% of single WR stars have a significant wind asymmetry, with an equator:pole density ratio of 2–3 being typical. It was postulated that the asymmetries stemmed from rapid rotation, and that the line-effect stars represented the high velocity tail of the rotational distribution.

1.1. WR137 (HD192641): a dust producing WC+O star binary

The presence of absorption lines in the spectrum of WR137 (Smith 1968) has led to its classification as a binary (WC7+OB). A careful study of photographic spectra by Massey et al. (1981) showed no radial-velocity (RV) variations and they suggested that the star was either single or had a binary period of more than 2 years. Radial velocity measurements by Moffat et al. (1986) also displayed no orbital variability, and they concluded that the period must be greater than 2 years. Annuk (1991) reported RV variations from a 10-year (1980–1990) series of photographic spectra and found them to be consistent with a 12-year period. RV measurements obtained by Underhill (1992) over the period 1986–1991 yielded no detectable systematic RV variation, while a period of 5680d was derived by Annuk (1994) after combining RV measurements from several sources.

It has been shown that WR137 undergoes sporadic dust formation episodes (Williams et al. 1985, 1987). The 3.8μm flux from WR137 fell from 1975 to 1980 and then rose to a peak in 1985. The IR flux then fell steadily. Williams et al. (1987) proposed that WR137 is an eccentric binary with a period of 13 years (consistent with the RV observations of Annuk) and that the dust formation episodes occur at periastron, when the colliding winds of the WR and OB components produce suitable conditions for grain condensation, and Williams & van der Hucht (1994) predicted that the next IR maximum should occur in 1997. At maximum, the dust mass is approximately $10^{-8}\,\mathrm{M}_{\odot}$, while the formation rate is $\sim 10^{-7}\,\mathrm{M}_{\odot}\,\mathrm{yr}^{-1}$ which represents about 0.5% of the total mass-loss rate. The latest dust formation episode produced a maximum near-IR flux in 1997.6, consistent with a 13.1yr period (Williams 1999, private communication).

Photopolarimetry of WR 137 (Robert et al. 1989) showed a low level of variability when compared to the other Cygnus WR stars, a result which indicates that binary effects on the polarization are small (as might be expected given the large separation predicted by the 13.1yr period, but see Sect. 5) and that the wind is probably more homogeneous than those of its neighbours.

It was found in Paper I that the WC+OB binary WR 137 shows a strong line effect, indicative of a global wind asymmetry which may aid dust condensation. In order to examine the stability of the wind geometry, and to search for any systematic effects in the polarization spectrum resulting from binarity, we monitored WR 137 from 1993 to 1998 (a timespan which encompasses periastron passage). In the following sections we present the data, estimate the foreground polarization, and analyse the intrinsic polarization spectra. Finally we discuss our results with the aid of numerical models in the context of the dust formation episodes and the geometry of the system.

2. Observations and data reduction

Moderate resolution spectropolarimetric observations of WR137 were obtained with the ISIS dual-beam cassegrain spectrograph and polarimetry module on the 4.2-m William Herschel Telescope. The adopted observing procedure is detailed in Paper I. A variety of gratings and detector combinations were employed over the years, although the measured resolutions (2–5Å) were always sufficient to resolve the emission lines and their polarization morphology.

The initial CCD frame preparation (debiasing, flatfielding) was performed using the FIGARO package (Meyerdierks 1992). The polarization spectra were then extracted using software delevoped by us (Harries 1995) following the prescription detailed by Harries & Howarth (1996). The POLMAP package (Harries 1996) was used to calibrate the spectra, using polarized standard stars to calibrate the PA zero-point and observations through a 100% polarizing filter to remove the PA rotation caused by slight chromicity of the half-wave plate. Observations of the zero polarization standard star ζ Peg revealed that the instrumental polarization was less than 0.05%. The instrumental polarization vector was not subtracted from the observations, due to its small size and the uncertainties of determing this vector when using an alt-azimuth telescope.

Further low-resolution data were obtained by using the high-throughput dual-beam HPOL spectropolarimeter on the 0.9m telescope of the Pine Bluff Observatory (PBO) at the University of Wisconsin. The HPOL instrument consists of a heavily modified Boller & Chivens spectrograph, optimized for high precision (Nordsieck & Harris 1996). The instrument provides simultaneous spectrophotometry and spectropolarimetry over two possible wavelength ranges, 3200–6020Å and 5980–10500Å with a resolution of 8Å and 10Å respectively. Polarimetric modulation is produced below the slit by a rotating super-achromatic halfwave retarder. This waveplate mechanism features an active angle detent, repeatable to 0.01 degrees. It makes 8 stops stepping every 11.25 degrees. The beam is then collimated and split into two orthogonally polarized beams by a calcite polarizing beamsplitter (Wollaston prism). These beams are separated perpendicular to the dispersion. The two beams are subsequently dispersed by one of two color gratings and recorded by an achromatic camera which was specifically designed for this instrument. The camera is all-refractive, which eliminates vignetting and thus enhances the polarimetric stability. The image is focussed on a Reticon 400×1200 pixel CCD. The instrument employs 2 apertures allowing the detection of two polarized star spectra and two polarized sky spectra simultaneously. The system quantum efficiency is approximately 10 per cent.

The polarimetric calibration of HPOL is performed using observations of polarized and unpolarized standards. The po-

Table 1. A log of the observations of WR137. The phase (ϕ) is computed with respect to near-IR maximum flux (1997.6) assuming a 13.1y period. The Obs. column refers to the source of the data, either the William Herschel Telescope (W) or the Pine Bluff Observatory (P).

Date	JD (-2400000)	ϕ	Obs.	Wavelength range (Å)
1993 Jul. 25	49181	0.697	W	3625–10870
1994 Mar. 24	49436	0.750	W	5236–6940
1995 Aug. 17	49947	0.857	W	6173–6981
1996 Jul. 15	50280	0.927	P	3200–10440
1996 Jul. 30	50295	0.930	W	4483–7456
1996 Aug. 18	50314	0.934	W	5302–6807
1996 Aug. 21	50317	0.934	P	6012–10436
1996 Aug. 22	50318	0.934	P	3225–10436
1996 Aug. 30	50326	0.936	P	3201–10440
1996 Sep. 12	50339	0.939	P	3201–10440
1996 Oct. 4	50361	0.944	P	3201–10440
1997 Aug. 12	50673	0.009	W	5255–6743
1998 Aug. 10	51036	0.085	W	6369–6772

larimetric stability is well determined at 0.002 per cent and less than ± 0.03 degrees in PA, allowing an accurate correction for the instrumental polarization. Photometric flux calibration is determined from 2 to 3 flux standard observations taken per night. It should be noted that the absolute flux level is poorly known due to non-photometric skies. However the broadband colours within either grating are accurate to better than 0.05 magnitudes (the 6×12 arcsecond slit being large enough to permit the entire stellar image to be passed to the spectrograph). Relative fluxes below 3600Å and above 9000Å can be substantially worse however due to extinction correction inaccuracies and nightly atmospheric water content variability.

A log of the observations is listed in Table 1, while the reduced spectra are plotted in Fig. 1. The line-effect is clearly seen in all the polarization spectra.

3. The interstellar polarization

All appreciably reddened stars will show some degree of interstellar polarization (ISP), caused by dichroic absorption by dust grains in the interstellar medium that are aligned by the Galactic magnetic field. Accurate estimation of the ISP is crucial to polarimetric analysis, since its magnitude often exceeds that of the intrinsic polarization vector.

Traditionally the ISP vector has been estimated from the polarization vectors of stars neighbouring the target: the field star method. This method is of limited use (see, for example, Fig. 1 of Robert et al. 1989 or Fig. 2 of Paper I), however, as it relies on two dubious assumptions, namely that the field stars are intrinsically unpolarized (the majority of field stars are B-type giants with unstable, and therefore possibly polarimetrically active, atmospheres) and that the Galactic magnetic field and the ISM are constant over small spatial scales. The problems of the field star method are exemplified in the neighbourhood of WR137, which displays a chaotic pattern (see Fig. 2(e) of Paper I). We therefore eschew the field star method and employ a more reliable (albeit model dependent) technique for determining the ISP: The continuum-to-line polarization vectors should point towards the interstellar vector when plotted in the QU plane. Thus by measuring the polarization in an emission line, and that of a nearby continuum region, one is able to estimate the ISP.

We chose to use the $\lambda 5805$ line for this analysis, since this line was observed at the majority of epochs and is strong enough to yield a good signal-to-noise in the line. We measured the polarization of the line and continuum using a 15Å bin centred on the line, and a nearby line-free bin (6000–6200Å). The results of the measurements are plotted in terms of q ($= Q/I$) and u ($= U/I$) in Fig. 2 along with the b-band photopolarimetry of Robert et al. (1989).

The direction of the intrinsic polarization is remarkably constant over the time of the observations (see Fig. 2), although there is evidence for continuum variability since the scatter in the continuum measurements (filled squares in Fig. 2) is greater than the errors on the individual measurements. If the continuum polarization vectors are distributed roughly evenly about the ISP point in QU-space then the continuum-to-line polarization vectors all point to a unique point, and the 'convergence method' may be used to obtain the ISP (see Harries et al. 1999). In this case the continuum-to-line polarization vectors are approximately parallel, and we must turn to an alternative method. Fortunately, the PBO data cover a large wavelength range, and we may determine the ISP by fitting a standard ISP law and intrinsic continuum spectrum to our dataset.

The wavelength dependence of the ISP is well modelled by the empirical Serkowski law, as modified by Whittet et al. (1992)

$$s_{\rm is}(\lambda) = s_{\rm max} \exp[-(0.01 + 1.66 \times 10^{-4}\lambda_{\rm max}) \ln^2(\lambda_{\rm max}/\lambda)] \quad (1)$$

where $s_{\rm is}(\lambda)$ is the normalized Stokes parameter (q or u) at wavelength λ, $s_{\rm max}$ is the maximum polarization which occurs at a wavelength $\lambda_{\rm max}$ (in Å).

The shape of the intrinsic continuum polarization is not known. Although electron-scattering is a grey process, competition between continuum opacity and electron-scattering opacity can lead to a slow decrease in polarization magnitude with increasing wavelength (see below). We therefore approximate the intrinsic continuum polarization by a linear expression

$$s_{\rm cont}(\lambda) = s_0 + p_1(\lambda - 5500) \quad (2)$$

where $s_{\rm cont}$ is the intrinsic continuum normalized Stokes parameter, and s_0 and p_1 are free parameters. This formalism assumes that the PA of the continuum polarization is a constant (a valid assumption providing that the scattering geometry is not a function of wavelength in the optical regime).

Harries et al. (1999) demonstrated that dilution dominates the line polarization morphology in the optical emission lines of WR stars, and so the intrinsic polarization goes as

$$s_{\rm int}(\lambda) = s_{\rm cont}(\lambda)/I(\lambda) \quad (3)$$

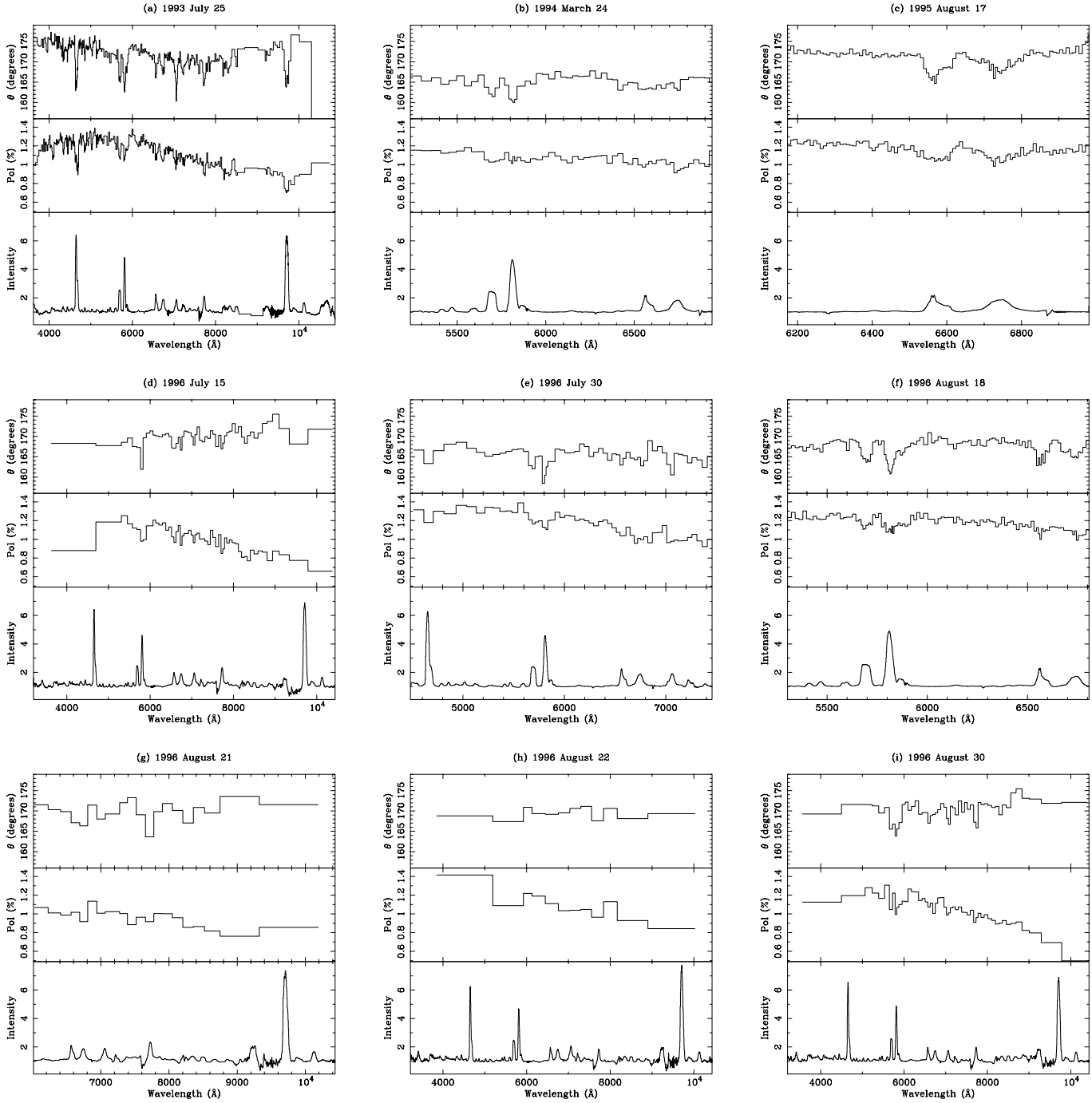

Fig. 1a–i. The spectropolarimetric data. The bottom panels shows rectified intensity, while the middle and upper panels show polarization magnitude and position angle respectively. All spectra are plotted with a constant error of 0.03% in polarization magnitude.

where $s_{\rm int}(\lambda)$ is the intrinsic normalized Stokes spectrum and $I(\lambda)$ is the rectified intensity spectrum. The observed polarization is then the vector sum of the intrinsic polarization and the ISP:

$$\mathbf{P}_{\rm obs}(\lambda) = \mathbf{P}_{\rm is}(\lambda) + \mathbf{P}_{\rm int}(\lambda). \quad (4)$$

We first rectified each of the spectra using low-order polynomial continuum fits to interactively defined line-free wavelength intervals, and edited out telluric spectral features. We then fitted Eq. (4) to the data using a weighted Marquardt minimization. Since the continuum polarization is variable we fitted for a single interstellar law plus separate continuum parameters for each spectrum.

The total number of free parameters comprised the three ISP law variables ($q_{\rm max}$, $u_{\rm max}$, $\lambda_{\rm max}$), plus three additional parameters (q_0, u_0, and p_1) for each spectrum. It was found that the fit converged very quickly to a solution with a reduced χ^2 of 1.18, and the parameters determined are listed in Tables 2

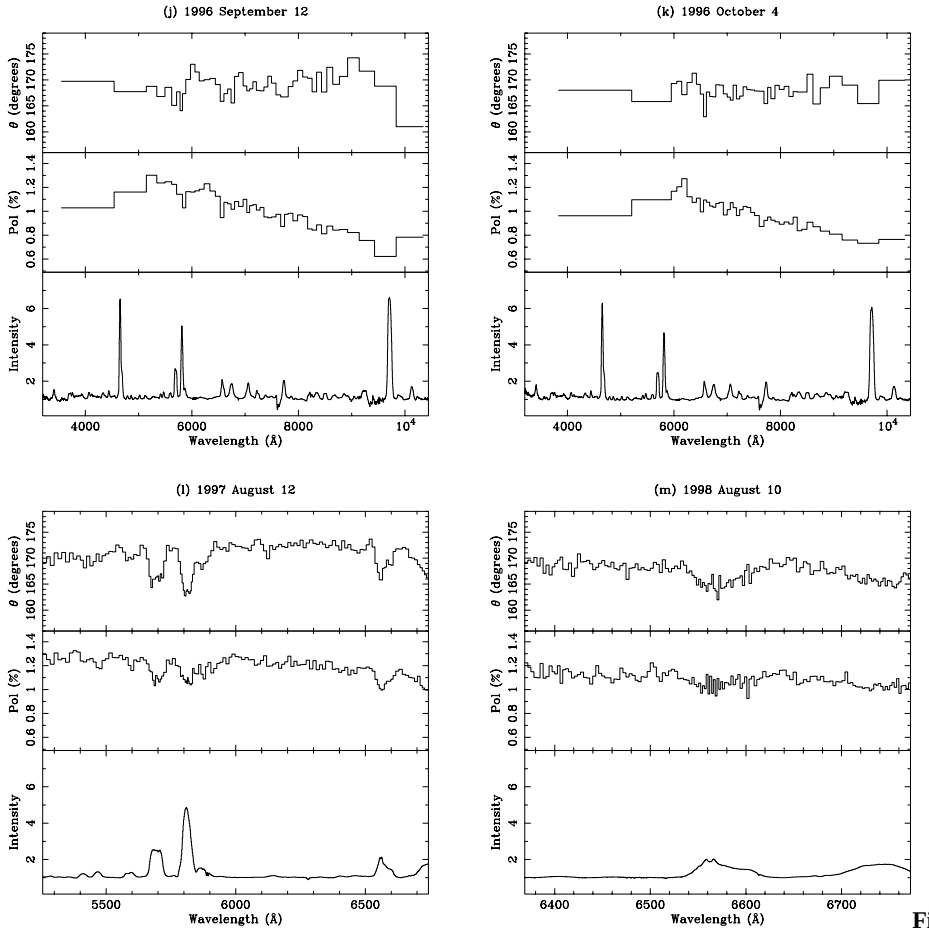

Fig. 1j–m.

Table 2. The interstellar polarization law derived from the fitting procedure.

Parameter	Value
$\overline{q}_{\max}$ (%)	$+0.80 \pm 0.01$
$\overline{u}_{\max}$ (%)	-0.64 ± 0.01
$\lambda_{\max}$ (Å)	5116 ± 21

Table 3. Continuum parameters from the least-squares fit.

Date	q_0 (%)	u_0 (%)	p_1 (10^{-6} Å^{-1})
1993 Jul. 25	0.43 ± 0.01	0.34 ± 0.01	-0.98 ± 0.02
1994 Mar. 24	0.20 ± 0.01	0.12 ± 0.01	-1.48 ± 0.40
1995 Aug. 17	0.42 ± 0.01	0.31 ± 0.01	-0.95 ± 0.26
1996 Jul. 15	0.26 ± 0.01	0.25 ± 0.01	-0.22 ± 0.10
1996 Jul. 30	0.37 ± 0.01	0.07 ± 0.01	-3.13 ± 0.14
1996 Aug. 18	0.37 ± 0.01	0.16 ± 0.01	-1.65 ± 0.17
1996 Aug. 21	0.22 ± 0.02	0.25 ± 0.03	-0.00 ± 0.25
1996 Aug. 22	0.39 ± 0.01	0.25 ± 0.01	-0.80 ± 0.13
1996 Aug. 30	0.33 ± 0.01	0.27 ± 0.01	-0.68 ± 0.07
1996 Sep. 12	0.29 ± 0.01	0.22 ± 0.01	-0.44 ± 0.10
1996 Oct. 4	0.27 ± 0.01	0.21 ± 0.01	-0.92 ± 0.11
1997 Aug. 12	0.42 ± 0.01	0.30 ± 0.01	-1.12 ± 0.12
1998 Aug. 10	0.56 ± 0.02	0.35 ± 0.02	-5.13 ± 0.16

and 3, while the ISP law is plotted in the QU plane in Fig. 2 [since we assume PA of the ISP law is constant with wavelength the ISP law traces out a straight line in QU space, which connects the minimum polarization $(0, 0)$ with the maximum $(+0.80, -0.64)$]. For completeness we also performed spectral fits adopting a quadratic form for the intrinsic polarization, which yielded an identical (to within errors) ISP law, as did fits assuming a flat continuum polarization, but with a significantly poorer fit quality.

Finally the ISP was subracted from each polarization spectrum in turn to yield the intrinsic polarization spectrum.

4. The intrinsic polarization

In Fig. 3 we plot the polarization magnitude and PA of the of the intrinsic spectra against wavelength. Although the p_1 parameter is negative for all the spectral fits (see Table 3), the decline of polarization magnitude with wavelength is very slow (particularly the PBO data, which have the longest wavelength coverage and therefore best constrain the p_1 parameter). This is consistent with our hypothesis that the dominant polarigenic source in the intrinsic spectra is electron scattering and Paper I it was found that the level of polarization observed is consistent with a geometry in which the equator:pole density ratio of the wind was approximately 2–3. The fact that the continuum polariza-

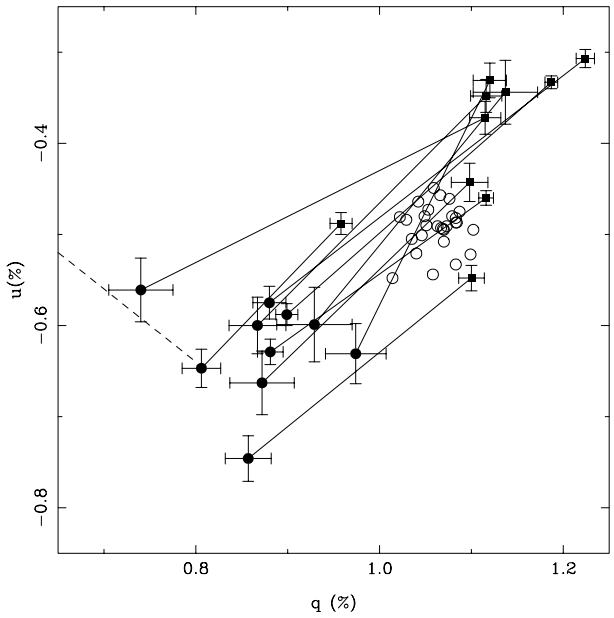

Fig. 2. The polarizations measured at the centre of $\lambda 5805$ (filled circles) are joined by solid lines to the continuum polarizations (filled squares) measured from the same spectrum. Photopolarimetry in the b-band (Robert et al. 1989) is plotted for comparison (open circles), although the presence of the strong 4650Å emission line complex in this passband renders a direct comparison with the new continuum measurements difficult. The dashed line represents the derived interstellar polarization law, connecting $(0, 0)$ to $(+0.85, -0.65)$.

tion decreases with wavelength would be consistent with the model proposed by Schulte-Ladbeck et al. (1992), in which the continuum thermalization radius grows as a function of wavelength, and gradually passes the $\tau_{es} = 1$ boundary, leading to a reduction in polarization magnitude as continuum photons 'see' a smaller free-electron column. Alternatively, the increase in polarization towards the blue could result from small-grain dust scattering (see Sect. 5).

It is probable that this density contrast plays a rôle in aiding the dust condensation process, and therefore that the asymmetric wind structure should be reflected in the dust distribution about the binary. Marchenko et al. (1999, hereinafter MMG99) used the NICMOS-2 instrument on the HST to image the dust emission from WR137 in the H' and K' bands in 1997 and 1998. Their 1998 K'-band image shows an extended (0.25 arcsec) lobe of emission to the east-southeast, and a clump to the west-northwest (see Fig. 4). It was shown that the PA of the observed polarization, as measured in Paper I, is roughly perpendicular to the elongated K'-band structure. We have demonstrated in Sect. 3 that the observed polarization is dominated by the interstellar component. The *intrinsic* polarization vector has a mean position angle of $17°$ (found by summing the intrinsic polarization spectra and measuring across 6375–6500Å, the only wavelength region common to all the spectra and devoid of strong emission lines), which is almost exactly perpendicular to the dust emission (Fig. 4). Hence the asymmetry close to the optical WR photosphere ($\sim 15 R_\odot$, Howarth & Schmutz 1992) is mirrored by that of the dusty region, approximately 10^4 times further away.

Although scattering in a flattened wind accounts for the majority of the intrinsic polarized flux, the continuum is variable and there must be additional scattering processes occuring. Short period WR+O binaries show a phase dependent intrinsic polarization, produced by the scattering of the O-star radiation in the wind of the WR component e.g. V444 Cyg (Robert et al. 1990) or CQ Cep (Harries & Hilditch 1997). Maximum polarization occurs at quadratures, when the angle between the binary line-of-centres and the observer is $90°$, and minimum polarization occurs at conjunctions. The polarization light curve therefore has maximum power in the second harmonic of the binary period, and details of the orbital geometry (the inclination, position angle of the line-of-nodes) may be recovered from a simple Fourier analysis (Brown et al. 1978).

We measured the intrinsic continuum polarization of our ISP-corrected spectra by summing the Stokes intensities over the spectral range 6375–6500Å. These measurements are plotted as a function of time and of binary phase (according to the IR light-curve with maximum light at $\phi = 0$ and a 13.1yr period) in Fig. 5. No correlation with binary phase is observed.

5. Numerical models

Since WR137 has a relatively long period the O-star radiation will be quite dilute in the region of the WR component, and it might be expected polarization variation will be small. In order to quantify any likely binary effects on the intrinsic polarization, and to check for consistency with our observations, we performed a numerical simulation of the scattering processes. We adopted a binary separation of 3×10^{14} cm, which is consistent with the radial velocity solution of Annuk (1994) and assuming $i \sim 90°$. The WR mass-loss rate ($\dot{M} = 8 \times 10^{-5} \mathrm{M}_\odot\ \mathrm{yr}^{-1}$) and terminal velocity ($v = 1960 \mathrm{km\,s}^{-1}$) were taken from Howarth & Schmutz (1992), and a luminosity ratio (L_{WR}/L_O) of 4 was estimated from the Howarth & Schmutz (1992) WC luminosity (5.4 dex in solar units) and that of a generic late-type O-star (4.8 dex, Howarth & Prinja 1989). We initially ignored the effects of the O star wind and populated the density grid assuming mass conservation, viz

$$\rho(r) = \frac{\dot{M}}{4\pi r^2 v} \tag{5}$$

where $\rho(r)$ is the density at distance r from the WR centre.

The continuum polarization produced by intra-binary scattering was computed by using the TORUS 3-D Monte-Carlo radiative transfer code (Harries 2000). Point photon sources were assumed, since the finite size of the stars will have a negligible effect on the polarization in such a wide system, and only electron-scattering opacity was considered. It was found that the polarization resulting from this model was less than 0.01%, considerably lower than the errors on our individual measurements, and an order of magnitude lower than the month-to-month variability observed in the intrinsic polarization.

We then considered the effects of wind-wind interaction on the intrinsic polarization. The collision between the O star wind

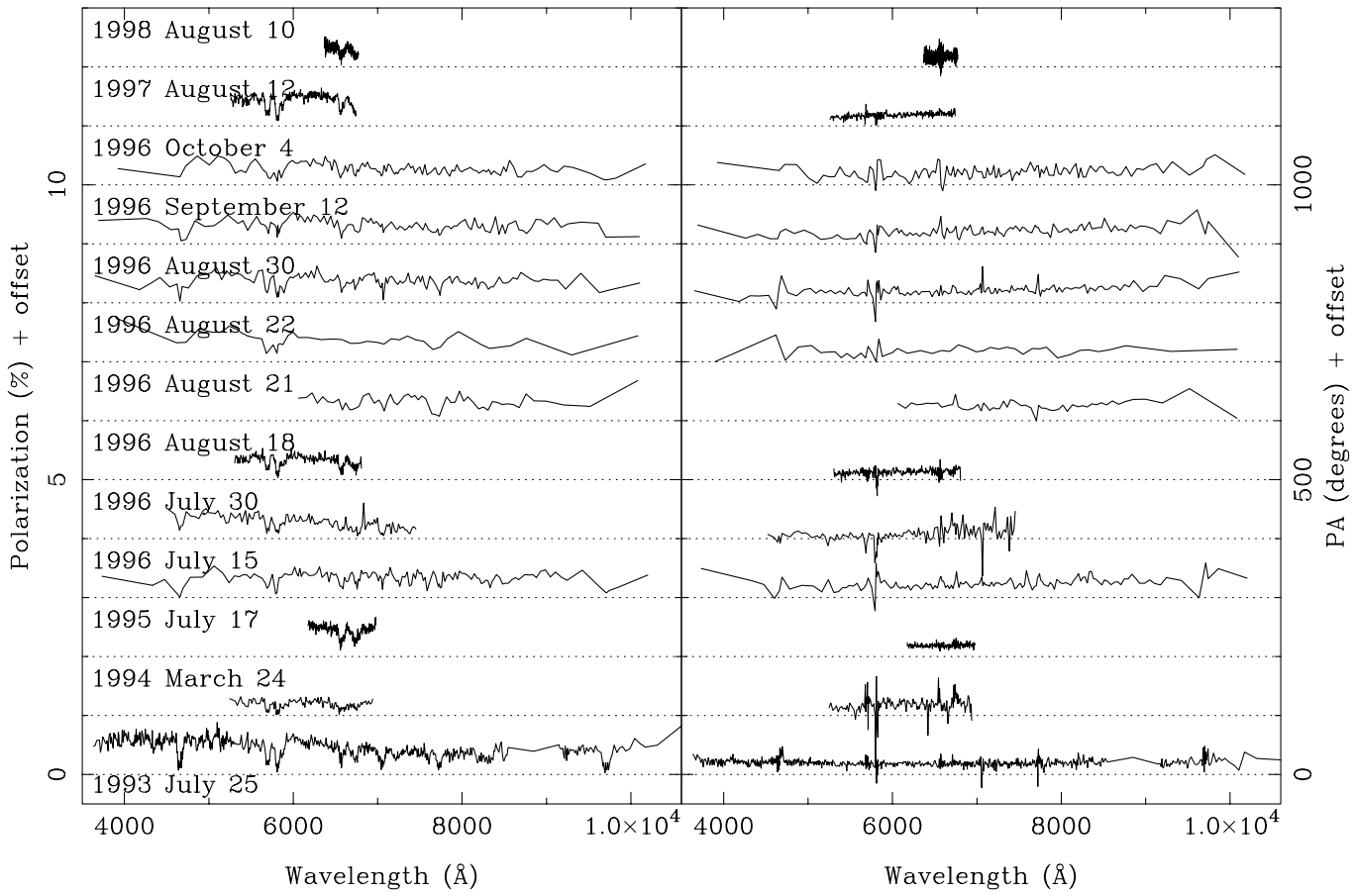

Fig. 3. The polarization magnitude (right-hand panel) and PA (left-hand panel) of the intrinsic spectra (binned to a constant error of 0.05%) plotted against wavelength. The dotted lines represent the zero polarization or PA level for the spectrum immediately above.

and the much stronger outflow from the WR star manifests itself as a curved interaction zone bounded by shocks. The shape of the interaction region is a function of the momentum ratio of the winds, and in the case of WR+O winds it is well-approximated by a cone. An analytical formula for the semi-opening angle (θ, in radians) of the cone was presented by Eichler & Usov (1993)

$$\theta = 2.1\left(1 - \frac{\eta^{2/5}}{4}\right)\eta^{1/3} \tag{6}$$

where

$$\eta = \frac{\dot{M}_{OB} v_{\infty,OB}}{\dot{M}_{WR} v_{\infty,WR}} \tag{7}$$

where η is typically in the range 0.01 to 0.1. The density of the post-shock flow is approximately 4 times that of the pre-shock wind.

For the first colliding wind simulation we adopted a value of $\eta = 0.1$ (giving an opening angle consistent with that estimated by MMG99), which gave a polarization of 0.03% at quadrature (polarization maximum). A marginally smaller value of 0.02% was found for a model computed with $\eta = 0.01$. These polarizations are approximately at the level of the errors on our individual measurements, and would be difficult to detect even if there were no other polarigenic sources. The orbital modulation of such a small signal will of course be swamped by any intrinsic variability resulting from the passage of density inhomogeneities through the wind or changes in the large-scale wind structure that is producing the majority of the polarized flux. We note that a lower mass-loss rate (as suggested by clumped wind models, e.g. Nugis et al. 1998) would tend to reduce the magnitude of the polarization.

If, as seems likely, the dust formation process is aided by the increase in local density arising from wind-wind collision then dust must be produced within a few binary separations of the WR+O system. The newly formed dust will therefore subtend a fairly large solid angle at the binary, and will intercept a substantial amount of the binary's flux. Mie scattering within this inherently asymmetric geometry will naturally lead to linear polarization, with its magnitude and direction placing strong constraints on the dust distribution close to the binary.

As we observe line depolarization, the scattering asymmetry producing the majority of the polarization must result from scattering in the vicinity of the $\tau_{es} = 1$ surface (although the amount of depolarization will depend on the details of the line formation process, with lines of high ionization species being produced closer to the continuum thermalization radius, and thus being more polarized than those produced further out in the wind). If

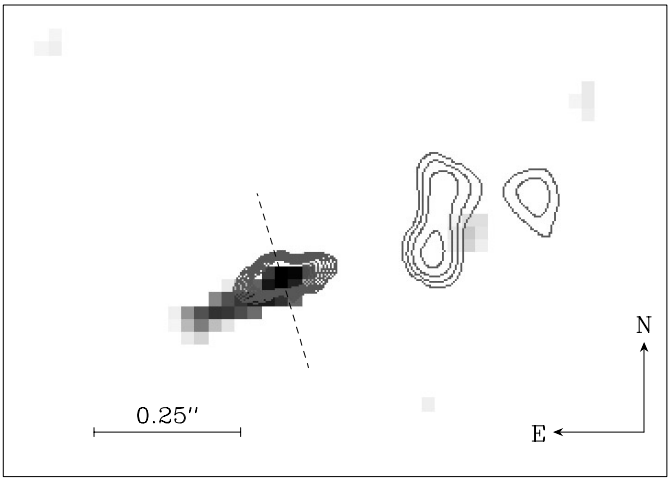

Fig. 4. The 1998 K' maximum-entropy restored image of WR137 (logarithmic grey-scale), and the 1997 image (contours) adapted from Fig. 3 of MMG99. The dashed line illustrates the position angle of the intrinsic polarization.

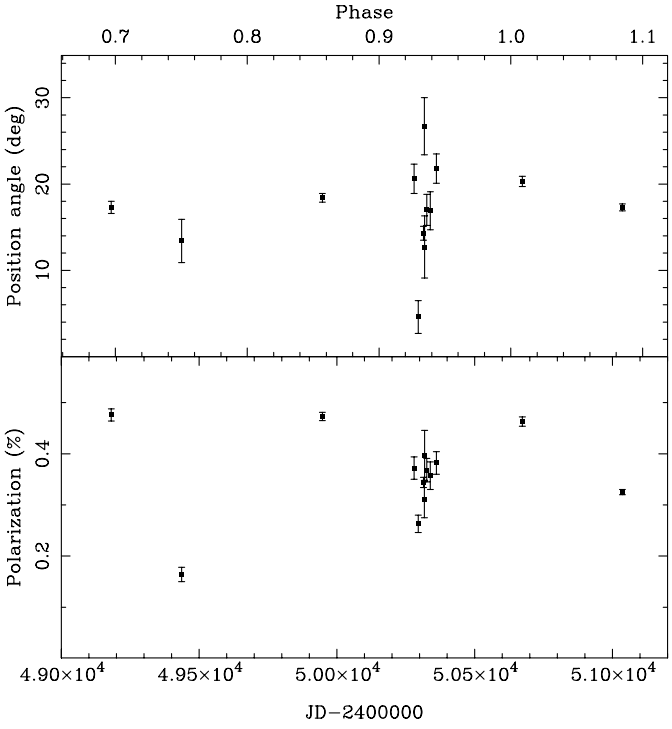

Fig. 5. The intrinsic continuum polarization as a function of Julian date (bottom axis) and IR phase (top axis).

the continuum polarization resulted from scatterings far from the star, in circumstellar dust for example, then we would not see line depolarization (the continuum and line flux would essentially see the same scattering geometry). As there are no discernable changes in the polarization vector as a function of phase, it appears that the polarization resulting from dust scattering must be negligible compared with the electron-scattered component. A viable model for dust formation in WR137 must therefore produce very little polarization.

Table 4. Results of the dust scattering model calculations. The columns are the mass-loss rate ($\dot{M}$, in units of 10^{-5}M$_\odot$ yr^{-1}), the binary separation (a), the total dust mass (M_{dust}), the optical depth of the dust (τ, measured along the binary line-of-centres), and the continuum polarization at 4000Å (p_{4000}). The values of optical depth and polarization are given for the 200Å maximum grain size, and also for the 500 Å maximum grain size (in brackets).

$\dot{M}$	a (10^{14} cm)	M_{dust} (10^{-8} M$_\odot$)	τ	p_{4000} (%)
1	1	5.4	2.9 (3.8)	0.17 (1.06)
	2	10.9	1.5 (1.9)	0.12 (1.34)
	4	21.7	0.7 (1.0)	0.07 (0.92)
	10	54.3	0.3 (0.4)	0.04 (0.47)
2	1	10.9	5.9 (7.7)	0.15 (0.82)
4	1	21.7	11.8 (15.4)	0.08 (0.16)
8	1	43.4	23.5 (30.7)	0.10 (1.73)

We adopted the dust distribution suggested by MMG99 as the basis for our scattering model. It is assumed that dust formation occurs in the conic volume enclosed by the wind-wind collision shock fronts, and that the observer–WR–cone angle is $90°$. The opening angle of this cone was estimated by MMG99 to be 40–60°, and they suggested that the dust production might occur within two binary separations out as far as 25 binary separations. [The resolution of the images meant that dust production closer to the binary could not be ruled out, although grain disruption by the UV radiation field would prevent dust formation at small distances.]

The composition of the dust is unknown, although Williams et al. (1990) found that amorphous carbon (AC) gave the best fit to the IR spectral energy distribution of WR140. The grain sizes are poorly constrained by observation, but models of grain growth suggest that the maximum likely size is 200Å (Zubko 1998). In the optical region and redwards these grains are small enough that the scattering occurs according to the Rayleigh scattering phase matrix. We used the laboratory refractive indices of Duley (1984) to compute the scattering and absorption Q factors for the grains, adopting a power-low distribution of grain sizes (index -3.5) with the smallest grain size set to 5Å.

In order to fully explore the parameter space (given the large uncertainties on the system parameters) we constructed a grid of dust scattering models. We calculated models for a range of binary separations from 10^{14} cm to 10^{15} cm, and a range of mass-loss rates from 1–8×10^{-5} M$_\odot$ yr^{-1}. Two maximum grain sizes were used: 200Å (the Zubko model) and 500Å (an arbitrary larger grain size–see below). The results of the computations are given in Table 4. The total mass of dust for all models is consistent with the constraints from the K-band images of MMG99 (2×10^{-7} M$_\odot$to within a factor of 3).

The values of p_{4000} in Table 4 correspond to the maximum polarization at that wavelength that can be produced by the model, as the majority of scatterings will be through $90°$; should the dust happen to be in front of the WR component, then no polarization will be observed since the geometry is circularly symmetric with respect to the observer's sightline. [Note that

since the optical depth scales with mass-loss rate and binary separation only the scattering geometry (and therefore the polarization) is idential for for models with the same value of $\dot{M}/a$].

All the models with the 200Å maximum grain size produce polarizations of between 0.1% and 0.2% at 4000Å (the polarization falls off rapidly with wavelength, reaching negligible values by 8000Å). It is possible that a level of 0.1% polarization by dust scattering is present in our dataset, although the variable nature of the continuum polarization on short time scales is unlikely to be due to dust formation episodes, which have a timescale of months. The presence of a small amount of polarization arising from dust scattering in the blue part of the spectrum would however be consistent with the negative values of the p_1 parameter.

It is interesting to note that should the dust grains be slightly larger (500Å), then the polarization produced by the dust distribution rises to $\sim 1\%$ due to the increase in the ratio of scattering to absorption efficiency ratio with grain size. Such a value is inconsistent with the observations, and we conclude that if the dust is being produced within a few binary separations, then the dust grain size distribution *must* be approximately consistent with the Zubko (1998) model.

In the absence of other polarigenic sources that are capable of producing the levels of observed polarization variability, we conclude that the bulk of this variation is attributable to electron-scattering by density inhomogeneites (clumps) in the wind of the WR component. The presence of these clumps is revealed via high-resolution, high-signal-to-noise spectroscopy, where they are seen as 'bumps' on emission line profiles, which accelerate both to the blue and red of the line centre (e.g. Lépine et al. 1996; Lépine & Moffat 1999).

6. Discussion

It appears that the WR component of WR137 has a flattened wind with an equator:pole density ratio of approximately 2–3 (Harries et al. 1999) and that this geometry is both stable over long timescales (as evidenced by the lack of variability in the position angle of the intrinsic polarization–see Fig. 3) and is aligned with the binary orbital plane (assuming that this plane is defined by the extended dust distribution observed by MMG99). The density enhancement must increase the rate of dust production over that expected from an isotropic wind, since more mass is being fed into the wind-wind collision volume than would otherwise be expected, but detailed analysis on the effects of the equatorially enhanced wind on the dust condensation process are beyond the scope of the current study.

It is clear that the homogenous dust distribution used in the numerical models is probably over-simplistic. Extremely high (milliarcsecond) resolution near-infrared images of the dusty nebulae around the dust producing WC+O binaries WR104 (Tuthill et al. 1999) and WR98a (Monnier et al. 1999) obtained by using aperture masking interferometry revealed Archimedian spiral structures, which were seen to rotate with the binary. The interpretation is that the spiral structures represent the wind-wind interaction zone– the dust 'nursery'. Future models of dust production, and radiative transfer, and these systems must attempt to include such complex geometries, and also a 'clumpy' distribution to the dust formation sites.

Two nitrogen-sequence WR stars that show the same spectropolarimetric structure as WR 137 are WR 6 and WR 134. These systems also display periodic variability in their emission line morphology, most likely resulting from the rotation of large-scale azimuthal wind structures (e.g. plumes) within their flattened outflows (St. Louis et al. 1995; Morel et al. 1998; McCandliss et al. 1994; Harries et al. 1999). The similarities between WRs 6 and 134, and WR 137 are striking and it is likely that these systems represent the most rapidly spinning WR stars, in which the radial line-driving force is in competition with rotational velocity fields. We note that the Hα+He II complex at 6560Å shows a double-peaked morphology at some phases (e.g. Fig. 1 *c* or *m*), an unusual spectroscopic morphology for WR stars, which is traditionally interpreted as resulting from line-formation in a rotating medium, such as a thin keplerian disk (see e.g. Underhill 1992). A search for rotationally modulated line-profile variability in WR 137 is urgently required in order to ascertain whether it is a carbon-sequence analogue of WRs 6 and 134, and this task is being undertaken by Marchenko and co-workers.

Acknowledgements. René Rütten is warmly thanked for performing the service observations at the WHT. We would like to thank the crew of observers who obtained the PBO data for this paper: William Ager, Michael Niebauer, and Nicolle Zellner. Marilyn Meade and John Wisniewski kindly assisted in the PBO data reduction. We are also grateful to Sergey Marchenko for providing his K-band image for Fig. 4 and for helpful comments on a draft of the paper, and Ian Howarth for useful discussions and obtaining one of the WHT spectra. We thank Peredur Williams for communicating his IR ephemeris, and Tony Moffat for a detailed and constructive referee's report. This research made use of the UCL node of the PPARC Starlink computer network.

References

Annuk K., 1991, In: van der Hucht K.A., Hidayat B. (eds.) Wolf-Rayet Stars and Inter-relations with Other Massive Stars in Galaxies, Kluwer, Dordrecht, p. 245
Annuk K., 1994, In: van der Hucht K.A., Williams P.M. (eds.) Wolf-Rayet Stars: Binaries, Colliding Winds, Evolution. Kluwer, Dordrecht, p. 231
Brown J.C., McLean I.S., Emslie A.G., 1978, A&A 68, 415
Crowther P.A., 1999, In: van der Hucht K.A., Koenigsberger G., Eenens P.R.J. (eds.) Wolf-Rayet Phenomena in Massive Stars and Starburst Galaxies. Proc. IAU Symp. No. 193, p. 116
Drissen L., St.-Louis N., Moffat A.F.J., Bastien P., 1987, ApJ 322, 888
Duley W.W., 1984, ApJ 287, 694
Eichler D., Usov V., 1993, ApJ 402, 271
Harries T.J., 1995, Ph.D. Thesis, University of London
Harries T.J., 1996, PPARC Starlink User Note No. 204
Harries T.J., 2000, MNRAS (in press)
Harries T.J., Howarth I.D., 1996, A&AS 119, 61
Harries T.J., Hilditch R.W., 1997, MNRAS 291, 544
Harries T.J., Howarth I.D., Hillier D.J., 1998, MNRAS 302, 499 (Paper I)

Harries T.J., Howarth I.D., Schulte-Ladbeck R.E., Hillier D.J., 1999, MNRAS 302, 499
Howarth I.D., Prinja R.K., 1989, ApJS 69, 527
Howarth I.D., Schmutz W., 1992, A&A 261, 503
Lépine S., Moffat A.F.J., 1999, ApJ 514, 909
Lépine S., Moffat A.F.J., Henriksen R.N., 1996, ApJ 466, 392
Marchenko S.V., Moffat A.F.J., Grosdidier Y., 1999, ApJ 522, 433 (MMG99)
Massey P., Conti P.S., Niemela V.S. 1981, ApJ 246, 145
McCandliss S., Bohannan B., Robert C., Moffat A.F.J., 1994, Ap&SS 221, 155
McLean I.S., Coyne G.V., Frecker J.E., Serkowski K., 1979, ApJ 228, 802
Meyerdierks H., 1992, PPARC Starlink User Note No. 86
Moffat A.F.J., Lamontagne R., Shara M.M., McAlister M., 1986, AJ 91, 1392
Monnier J.D., Tuthill P.G., Danchi W.C., 1999, ApJ 525, 97
Morel T., St.-Louis N., Moffat A.F.J., et al., 1998, ApJ 498, 413
Nordsieck K.H., Harris W., 1996, In: Roberge W.G., Whittet D.C.B., (eds.) ASP Conf. Ser. Vol. 97, Polarimetry of the Interstellar Medium. ASP, San Francisco, p. 100
Nugis T., Crowther P.A., Willis A.J., 1998, A&A 333, 596
Robert C., Moffat A.F.J., Bastien P., Drissen L., St.-Louis N., 1989, ApJ 347, 1034
Robert C., Moffat A.F.J., Bastien P., St.-Louis N., Drissen L., 1990, ApJ 359, 211
Schulte-Ladbeck R.E., 1994, Ap&SS 221, 347
Schulte-Ladbeck R.E., Nordsieck K.H., Taylor M., et al., 1992, ApJ 387, 347
Smith L.F., 1968, In: Gebbie K.B., Thomas R.N. (eds.) Wolf-Rayet Stars. NBS Special Pub. 307, p. 23
St.-Louis N., Drissen L., Moffat A.F.J., Bastien P., 1987, ApJ 322, 870
St.-Louis N., Dalton M.J., Marchenko S.V., Moffat A.F.J., Willis A.J., 1995, ApJ 452, 57
Tuthill P.G., Monnier J.D., Danchi W.C., 1999, Nat 398, 487
Underhill A.B., 1992, ApJ 398, 636
Whittet D.C.B., Martin P.G., Hough J.H., et al., 1992, ApJ 386, 562
Williams P.M., van der Hucht K.A., 1994, In: The Impact of Long-Term Monitoring on Variable Star Research. Kluwer, Dordrecht
Williams P.M., van der Hucht K.A., Thé P.S., 1987, QJRAS 28, 248
Williams P.M., Longmore A.J., van der Hucht K.A., et al., 1985, MNRAS 215, 23p
Williams P.M., van der Hucht K.A., Pollock A.M.T., et al., 1990, MNRAS, 243, 662
Willis A.J., 1999, In: van der Hucht K.A., Koenigsberger G., Eenens P.R.J. (eds.) Wolf-Rayet Phenomena in Massive Stars and Starburst Galaxies. Proc. IAU Symp. No. 193, p. 1
Zubko V.G., 1998, MNRAS 295, 109